Accepted for publication in Journal of Biomechanics (Jan. 27, 2010)

Aerodynamic study of different cyclist positions: CFD analysis and full-scale wind-tunnel tests

Thijs Defraeye [a, *], Bert Blocken [b], Erwin Koninckx [c], Peter Hespel [c] and Jan Carmeliet [d,e]

[a] *Laboratory of Building Physics, Department of Civil Engineering, Katholieke Universiteit Leuven, Kasteelpark Arenberg 40, 3001 Heverlee, Belgium*
[b] *Building Physics and Systems, Eindhoven University of Technology, P.O. Box 513, 5600 Eindhoven, The Netherlands*
[c] *Research Centre for Exercise and Health, Department of Biomedical Kinesiology, Katholieke Universiteit Leuven, Tervuursevest 101, 3001 Heverlee, Belgium*
[d] *Chair of Building Physics, Swiss Federal Institute of Technology Zurich (ETHZ), Wolfgang-Pauli-Strasse 15, 8093 Zürich, Switzerland*
[e] *Laboratory for Building Science and Technology, Swiss Federal Laboratories for Materials Testing and Research (Empa), Überlandstrasse 129, 8600 Dübendorf, Switzerland*

Keywords

CFD, drag, cyclist, aerodynamics, wind tunnel

Word count (Introduction to acknowledgements): 3586 words

Submission as an Original Article

[*] Corresponding author. Tel.: +32 (0)16321348; Fax: +32 (0)16321980.
E-mail address: thijs.defraeye@bwk.kuleuven.be

Abstract
Three different cyclist positions were evaluated with Computational Fluid Dynamics (CFD) and wind-tunnel experiments were used to provide reliable data to evaluate the accuracy of the CFD simulations. Specific features of this study are: (1) both steady Reynolds-averaged Navier-Stokes (RANS) and unsteady flow modelling, with more advanced turbulence modelling techniques (Large-Eddy Simulation - LES), were evaluated; (2) the boundary layer on the cyclist's surface was resolved entirely with low-Reynolds number modelling, instead of modelling it with wall functions; (3) apart from drag measurements, also surface pressure measurements on the cyclist's body were performed in the wind-tunnel experiment, which provided the basis for a more detailed evaluation of the predicted flow field by CFD. The results show that the simulated and measured drag areas differed about 11% (RANS) and 7% (LES), which is considered to be a close agreement in CFD studies. A fair agreement with wind-tunnel data was obtained for the predicted surface pressures, especially with LES. Despite the higher accuracy of LES, its much higher computational cost could make RANS more attractive for practical use in some situations. CFD is found to be a valuable tool to evaluate the drag of different cyclist positions and to investigate the influence of small adjustments in the cyclist's position. A strong advantage of CFD is that detailed flow field information is obtained, which can not easily be obtained from wind-tunnel tests. This detailed information allows more insight in the causes of the drag force and provides better guidance for position improvements.

1. Introduction

The performance of cyclists is strongly affected by the resistance they experience, which consists of aerodynamic resistance or drag, rolling resistance, wheel-bearing and drive-train friction and road gradient. At high speeds (≈ 50 km/h), the majority of this resistance, about 90% or more, is caused by aerodynamic drag (Grappe et al., 1997; Kyle and Burke, 1984). The largest part of this aerodynamic resistance, namely about 60 - 70%, is accounted for by the cyclist's body (Gross et al., 1983; Kyle and Burke, 1984).

The aerodynamic drag of a cyclist originates from viscous drag, which is caused by skin friction in the boundary layer on the cyclist's surface, and form drag, which is related to the shape of the cyclist. Viscous drag can be reduced by lowering the surface roughness, for example by wearing a smooth suit or by shaving the skin. However, for bluff bodies such as cyclists, form drag usually is the most important contributor to drag (> 90% in this study). Form drag can be reduced by streamlining the cyclist, hence reducing the wake flow downstream of the cyclist, and by reducing his frontal area. Thereby, form drag is in essence related to the position of the cyclist on the bicycle, although it can also be reduced by improving the aerodynamics of his equipment, e.g. by wearing an aerodynamic helmet.

Previous research by field testing and wind-tunnel experiments (Broker, 2003; Garcia-Lopez et al., 2008; Grappe et al., 1997; Jeukendrup and Martin, 2001) showed that adjustments to the cyclist's position, even minor ones, can result in a decrease of the aerodynamic drag, which indicates the possibility for optimisation. Therefore, these techniques have been frequently used to improve the position of elite cyclists. Note however that improving the position from an aerodynamic point of view does not necessarily result in optimised metabolic cost and respiratory functions. In terms of race performance, the optimal position is therefore usually a compromise between power output and aerodynamics. Such aerodynamic adjustments are usually assessed empirically (by trial and error) based on the reduction in drag force but are rarely related to the analysis of changes in the flow field, e.g. reduction of the wake flow, which lead to the actual drag improvements. The primary reason is that measurements of the flow field are less straightforward and more time-consuming compared to drag measurements. Usually, the spatial resolution is also too limited to represent the complex flow field around the cyclist in detail, such as the locations of boundary-layer separation. An appropriate tool to provide good insight in the flow field around the cyclist is Computational Fluid Dynamics (CFD), which provides very high resolution data of the flow field together with drag information, also allowing for a separate quantification of form drag and skin-friction drag. It has already been used to evaluate aerodynamics in different sport disciplines, like swimming (Bixler et al., 2007; Bixler and Riewald, 2002; Bixler and Schloder, 1996; Gardano and Dabnichki, 2006; Lecrivain et al., 2008; Rouboa et al., 2006; Zaïdi et al., 2008), soccer (Barber et al., 2009), bobsleighing (Dabnichki and Avital, 2006), ski jumping (Meile et al., 2006) and cycling (Hanna, 2002; Lukes et al., 2004). There is however still room for improvement regarding some CFD modelling issues: (1) In most studies, except that of Rouboa et al. (2006) and Lecrivain et al. (2008), steady flow modelling was used; (2) Reynolds-averaged Navier-Stokes (RANS) modelling is used, usually with the standard k-ε turbulence model. The k-ε model however often leads to unsatisfactory flow modelling for bluff bodies (Casey and Wintergerste, 2000), especially in the wake; (3) Wall functions are used to model the boundary layer, except by Barber et al. (2009). Wall functions can however result in inaccurate predictions of wall friction and boundary-layer transition from a laminar to a turbulent boundary layer (Casey and Wintergerste, 2000); (4) 2D modelling is used in some studies (Rouboa et al., 2006; Zaïdi et al., 2008); (5) If CFD validation is performed, usually only drag is considered and comparison of flow quantities, i.e. velocities or surface pressures, is generally not performed.

The aim of this study is to evaluate the use of CFD for the analysis of aerodynamic drag of different cycling positions and to examine and improve some of the mentioned limitations of previous CFD modelling studies for sport applications. Steady RANS and (unsteady) Large-Eddy Simulation (LES) turbulence modelling techniques are compared where the boundary layer on the cyclist's surface is resolved entirely, instead of being modelled by wall functions. For CFD evaluation purposes, wind-tunnel experiments on a full-scale cyclist were carried out for three cyclist positions. Apart from drag measurements, also surface pressure measurements on the cyclist's body were performed to allow evaluation of the predicted flow field of CFD to some extent. In order to compare the obtained drag coefficients from wind-tunnel experiments and CFD with those of previous studies, a brief overview and discussion on this previous work is given in the next section.

2. Aerodynamic drag predictions

Aerodynamic drag is usually quantified by defining a dimensionless drag coefficient C_D, which relates the drag force F_D (N) to the frontal area A (m^2):

$$F_D = AC_D \frac{\rho U^2}{2} \quad (1)$$

where ρ is the density of air (kg/m^3) and U is the approach flow wind speed (m/s). Often, the drag area (AC_D) is reported instead of C_D, since it does not require an explicit determination of A. Aerodynamic drag has been quantified using different techniques, including wind-tunnel tests. Compared to other techniques, wind-tunnel tests are often costly and differ from reality (i.e. the outdoor environment) in several aspects: (1) The continuous variation of wind speed and wind direction is not accounted for; (2) The turbulence level is usually very low compared to the outdoor environment, since mostly low-turbulence wind tunnels are used, which can have an influence on the location of the boundary-layer separation points on the cyclist's surface. Note that boundary-layer wind tunnels can account for much higher turbulence levels in the approach flow; (3) Mostly "static" cyclists were considered, i.e. without pedalling and rotating wheels; (4) The boundary layer on the lower wind-tunnel wall, on which the bicycle is usually mounted, is not present in reality if there is no wind; (5) The rolling resistance is not taken into account. On the other hand, wind-tunnel tests allow for good flow conditioning and highly accurate, reliable measurements, resulting in a high sensitivity to small adjustments to the cyclist's position. A non-exhaustive summary of the obtained drag areas and the experimental details for previous wind-tunnel research is given in Table 1. For an overview of other measurement techniques and related drag coefficients, the reader is referred to Garcia-Lopez et al. (2008), Grappe et al. (1997) and Lukes et al. (2005).

A significant spread can be found on the results in Table 1, even for cyclists in the same position: an average value of 0.23 for the time-trail position with a standard deviation of 0.03. This spread is attributed to differences in the experimental setups: (1) Cyclists have different anthropometric characteristics. Some experiments tried to account for this by considering a number of cyclists; (2) A specific bicycle is used (frame and wheels) with specific settings, e.g. handlebar height, which depends on the cyclist; (3) Different cycling equipment, i.e. helmets, clothing, glasses and shoes, is used; (4) Possible Reynolds number effects could play a role due to the use of different wind speeds although C_D is usually fairly constant in the Reynolds number range for cycling (Basset et al., 1999); (5) "Static" and "dynamic" cyclists are considered whereas sometimes significant differences were found between both approaches (Garcia-Lopez et al., 2008). The term "dynamic" indicates that pedalling and/or rotating wheels are taken into account, while they are both not taken into account for a "static" cyclist; (6) The blockage ratio of some tunnels, i.e. the ratio of frontal area of cyclist to area of the test section, is not negligible which usually leads to an overestimation of C_D. Note that even a higher variability exists if also results obtained with other measurement techniques are included (see Grappe et al., 1997).

3. Methods

3.1. Experimental setup

The experiments were carried out in a closed-circuit wind tunnel (Dutch-German Wind tunnels, Marknesse, The Netherlands). The test section was 2.25 m high and 3 m wide. A standard racing bicycle (Soloist Team – Cervélo SA, Switzerland) with disc wheels and a standard handlebar was mounted in the test section on a bicycle stand (Figure 1), with both wheels fixed. Since the velocity profile in the test section was uniform, except for the thin boundary layers on the walls, the stand was placed on a round plate, at 0.1 m from the lower wind-tunnel wall, for the bicycle to be outside of the boundary layer on this wall, since this boundary layer is also not present in reality, i.e. on the road surface, if there is no wind flow. A positioning system for the cyclist was mounted on the bicycle in order to ensure that the cyclist's position was kept constant during the tests and that this position was reproducible for 3D scanning afterwards. Three different "static" positions, i.e. without pedalling, were investigated (Figure 2), namely the upright position (UP), the dropped position with straight arms (DP) and the time-trail position (TTP). For the time-trail position, a time-trail handlebar was mounted. For all cyclist positions, the wind direction was parallel to the bicycle axis, representing a head wind. The frontal areas for these positions are respectively 0.41, 0.37 and 0.34 m^2. The maximal blockage ratio was obtained for the upright position and

was 6%. The height and the weight of the cyclist were 183 cm and 72 kg respectively. He was equipped with an aerodynamic helmet, glasses, gloves and a standard racing suit with long sleeves (not shown in Figure 2).

Measurements were carried out at three wind speeds, namely 10, 15 and 20 m/s, in order to identify possible Reynolds number effects. The turbulence intensity at the inlet of the test section was 0.02%. The drag force, i.e. the horizontal component parallel to the wind direction and bicycle, was measured using a force transducer with a precision of 0.05 N, i.e. 0.0008 m² for the drag area AC_D at 10 m/s (± 0.5%). The data were sampled at 10 Hz for 25 s. Surface pressures on the cyclist's body were measured using 30 small pressure plates with an accuracy of 7 Pa (0.1% of total range). The locations of these pressure plates are shown schematically in Figure 3. The pressures were sampled at 1 Hz for 40 s. The work was approved by the local ethics committee related to the institution and the cyclist gave informed consent to the work before starting the study.

3.2. Numerical simulations

A digital model of the cyclist was obtained for every position using a high-resolution 3D laser scanning system (K-Scan, Nikon Metrology, Belgium), capturing the specific body characteristics of the cyclist. For meshing purposes, surfaces details were smoothed out to some extent and the bicycle, the bicycle stand, the cyclist positioning system and the round plate were not included in the computational model. This virtual cyclist was placed in a computational domain, representing the wind tunnel. The size of the computational domain and the imposed boundary conditions are specified in Figure 4. For the CFD simulations, steady RANS is used with the standard k-ε turbulence model (Launder and Spalding, 1972) and with low-Reynolds number modelling (LRNM), which is used to resolve the boundary layer on the cyclist's surface. Unsteady LES is also evaluated. Additional information on the CFD simulations can be found in Appendix 1.

4. Results and discussion

4.1. Wind-tunnel experiments: Drag area

The drag areas of the cyclist (with and without bicycle), obtained by the wind-tunnel experiments, are reported in Table 2 for the three positions at 10 m/s. Note that the drag areas of the cyclist without bicycle are obtained by subtracting the drag area of the bicycle setup itself (which includes bicycle, bicycle stand, round plate and positioning system, see Figure 1), which was measured separately, from the combined drag area of the cyclist and the bicycle setup. This is a rather simplified way of obtaining the drag area of the cyclist since in reality the cyclist himself will influence the drag of the bicycle setup to some extent, which is called interference drag. The drag areas of the cyclist with the bicycle are obtained in a similar way. The percentage of the drag area of the cyclist to the total drag area of cyclist and bicycle is also reported in Table 2. No distinct Reynolds number effects were noticed at higher wind speeds.

The results confirm that reducing the frontal area of the cyclist can significantly reduce his drag area. As expected, the aerodynamic drag of the cyclist is indeed 60-70% of the total drag. For all cyclist positions, a relatively low drag area is obtained (cyclist with bicycle) in the wind-tunnel experiment: in the TTP, a value of 0.211 m² is found, compared to an average value of 0.23 m² in previous wind-tunnel experiments (Table 1).

4.2. CFD simulations

The drag areas obtained by the wind-tunnel experiments, for the cyclist without bicycle setup (see Table 2), are compared with the results from the CFD simulations with RANS and LES in Table 3 for the three cyclist positions. For all positions, the accuracy of LES is equal to or higher than RANS, which is probably due to a better prediction of the wake flow. The systematically higher drag areas found for CFD, compared to wind-tunnel data, could be attributed to several reasons: (1) Only the cyclist is modelled in the CFD simulations and thereby the interference drag with the bicycle setup is not accounted for; (2) The CFD simulations are performed assuming a perfectly smooth cyclist surface, since surface roughness cannot be specified if LRNM is used to model the boundary layer. In the wind-tunnel experiment however, the cyclist's surface was not perfectly smooth due to the cyclist's clothing. As a result, the predicted skin-friction drag should be lower in the CFD simulations. Since it is only a small percentage of the total drag for bluff bodies, namely about 5% in this study (predicted by CFD simulations), the resulting decrease of the total drag will be limited and could even not be noticed: the total drag area obtained with CFD is actually higher than the wind-tunnel data. More important however is the fact that surface roughness could alter the locations where boundary-layer separation occurs on the cyclist's surface by which the flow field around the cyclist will change and therefore also the resulting form drag. Under appropriate conditions, a boundary layer could remain more attached on a rough surface (i.e. in the wind tunnel in this study) by which the wake zone and therefore also the total drag are reduced (Wilson, 2004). This could explain why the "smooth" cyclist of CFD exhibits a systematically higher drag area; (3) The surface details of the cyclist (e.g. eyes or nose) are smoothed out to some extent in the computational model; and (4) Even very sophisticated turbulence modelling techniques, like LES, still always "model" (i.e. approximate instead of solve) some parts of the turbulent flow, by which there will inherently be a difference with the actual flow conditions,

most likely in the wake of the cyclist. As argued above however, the discrepancies are not only related to turbulence modelling but also to simplifications to the computational model.

In Figure 5 and 6, the C_P coefficients obtained with the wind-tunnel experiments are compared to the results from the CFD simulations, for RANS and LES (time-averaged C_P values), for the UP and TTP positions. The C_P coefficient is defined as:

$$C_P = \frac{(p_{surf} - p_{inl})}{\frac{\rho U^2}{2}} \tag{2}$$

where p_{surf} is the static pressure on the cyclist's body and p_{inl} is the static pressure at the inlet of the wind-tunnel test section. For the CFD simulations, p_{inl} is the average pressure at the inlet of the computational domain. Note however that this inlet is not located at the same location as the inlet of the wind-tunnel test section, which is done to limit the size of the upstream part of the computational domain. As expected, an overpressure is found on the front side of the cyclist, leading to positive C_P values, whereas in the wake of the cyclist, negative C_P values are found. Note that the C_P values, obtained in the wind tunnel, are reported for 20 m/s in Figure 5 and 6 since the relative accuracy of the C_P values is higher at high wind speeds. The use of these C_P values instead of those at 10 m/s can be justified since no significant Reynolds number effects were noticed. Since the location of the pressure sensors could not be determined exactly, the reported CFD data are actually the averaged pressures within a circular zone (radius 2.5 cm) on the surface of the cyclist. The uncertainty band for the CFD results is the standard deviation from this averaged value. For the uncertainty of the wind-tunnel data, the measurement error on the pressure plates (7 Pa) is used, which is larger than the standard deviation on C_P for almost all points. The numbers of the sensors (see Figure 3), where the differences between wind-tunnel data and CFD are significant, are indicated in Figure 5 and 6. Note that a good agreement of CFD with wind-tunnel measurements implies that the data are all located near the solid line which is shown in the figures. The dotted lines represent 25% deviation from this solid line.

A good to very good agreement is found for most pressure plates for both cyclist positions and for both RANS and LES, especially for the TTP position. Note that the points that show the largest discrepancies are those on the side of the cyclist (points 27-30). This is the case for both cyclist positions. At these points, the CFD simulations predict too high negative pressure coefficients. This again could be a result from the difference in the location of the separation points, which is indicated by a larger underpressure for CFD, where boundary-layer separation seems to occur faster. Distinct outliers are also found at points 3, 4 and 8 for the UP position and at point 10 for the TTP position. Especially, the lower C_P value for point 3 in the wind-tunnel experiment has an obvious cause, namely the fact that this point is in the wake of a part (slender beam) of the bicycle setup (Figure 2a).

If the RANS and LES simulation results are compared, it is clear that LES provides a higher accuracy, both for drag and surface pressures. The much larger computational cost of LES compared to steady RANS, i.e. about one order of magnitude, and the additional temporal sensitivity analysis that is required however makes it much less attractive for practical calculations.

Despite the (small) differences between CFD and wind-tunnel results, the main advantage of CFD is that detailed flow field information is obtained, which allows more insight into the causes of the drag force, e.g. the wake flow, and which provides better guidance for position improvements. Note however that it is difficult to obtain an "absolute" optimum rider positioning by means of wind-tunnel tests or CFD simulations since both optimisation approaches will always differ to some extent from reality (see Section 2), which is dependent on the environmental conditions, the size of the group in which the cyclist is riding and his position with respect to the others, etc. Different "optimal" positions can therefore be found, depending on the specific conditions.

5. Conclusions

In this study, the drag areas obtained by wind-tunnel experiments showed good agreement with previous experiments. The CFD simulations predicted the drag areas with an accuracy of about 11% for RANS and about 7% for LES, which is considered to be a close agreement in CFD studies. A relatively good agreement was also obtained for the C_P values, especially for the aerodynamic position and when using LES (for all positions). The C_P measurements allowed for a more in depth comparison of RANS and LES than only the drag areas. The discrepancies between CFD and wind-tunnel data were not entirely related to limitations of the turbulence modelling itself but were also attributed to simplifications made in the computational model. Regarding the turbulence modelling, LES is found to provide more accurate flow predictions than RANS, but the increased computational cost does not always justify this increased accuracy. This study has shown that CFD is a valuable alternative to evaluate the drag of different cyclist positions with sufficient accuracy and to investigate the influence of small adjustments in cyclist positions. Its main advantage is that detailed flow field information is obtained, which allows more insight in the causes of the drag force and provides better guidance for position improvements.

Conflict of interest statement

The authors of the manuscript entitled "Aerodynamic study of different cyclist positions: Full-scale wind-tunnel tests and CFD analysis" do not have any conflict of interest.

Acknowledgements

This study was funded by the Flemish Government and the Flemish Cycling Federation. These sponsors had no involvement in: the study design, in the collection, analysis and interpretation of data; in the writing of the manuscript; and in the decision to submit the manuscript for publication. Special thanks goes to Jos Smets, Director of Sport at the Belgian Cycling Federation, for his enduring interest and support to integrate innovation in cycling. In addition, the high-quality assistance of the DNW team, headed by Ir. Eddy Willemsen, for the wind-tunnel tests is gratefully acknowledged.

References

Barber, S., Chin, S.B., Carre, M.J., 2009. Sports ball aerodynamics: A numerical study of the erratic motion of soccer balls. Computers & Fluids 38 (6), 1091-1100.

Basset, D.R., Kyle, C.R., Passfield, L., Broker, J.P., Burke, E.R., 1999. Comparing cycling world hour records, 1967-1996: modeling with empirical data. Medicine and Science in Sports and Exercise 31 (11), 1665-1676.

Bixler, B., Pease, D., Fairhurst, F., 2007. The accuracy of computational fluid dynamics analysis of the passive drag of a male swimmer. Sports Biomechanics 6 (1), 81-98.

Bixler, B., Riewald, S., 2002. Analysis of a swimmer's hand and arm in steady flow conditions using computational fluid dynamics. Journal of Biomechanics 35 (5), 713-717.

Bixler, B., Schloder, M., 1996. Computational fluid dynamics. An analytical tool for the 21st century swimming scientist. Journal of Swimming Research 11, 4-22.

Broker, J.P., 2003. Cycling power: Road and mountain. In: Burke, E.R. (Ed.), High-Tech Cycling: The Science of Riding Faster. Human Kinetics, Colorado, pp. 147-174.

Broker, J.P., Kyle, C.R., 1995. Pursuit Aerodynamics, Project 96: Wind tunnel test results. USOC Sport Science and Technology Report, Colorado Springs, pp. 1-46. (from Basset et al., 1999)

Casey, M., Wintergerste, T., 2000. Best Practice Guidelines. ERCOFTAC Special Interest Group on "Quality and Trust in Industrial CFD", ERCOFTAC.

Dabnichki, P., Avital, E., 2006. Influence of the position of crew members on aerodynamics performance of a two-man bobsleigh. Journal of Biomechanics 39 (15), 2733-2742.

Dal Monte, A., Leonardi, L.M., Menchinelli, C., Marini, C., 1987. A new bicycle design based on biomechanics and advanced technology. International Journal of Sport Biomechanics 3, 287-292.

Defraeye, T., Blocken, B., Carmeliet, J., 2010. CFD analysis of convective heat transfer at the surfaces of a cube immersed in a turbulent boundary layer. International Journal of Heat and Mass Transfer 53 (1-3), 297-308.

Garcia-Lopez, J., Rodriguez-Marroyo, J.A., Juneau, C.E., Peleteiro, J., Martinez, A.C., Villa, J.G., 2008. Reference values and improvement of aerodynamic drag in professional cyclists. Journal of Sports Sciences 26 (3), 277-286.

Gardano, P., Dabnichki, P., 2006. On hydrodynamics of drag and lift of the human arm. Journal of Biomechanics 39 (15), 2767-2773.

Gibertini, G., Campanardi, G., Grassi, D., Macchi, C., 2008. Aerodynamics of biker position. In Proceedings of BBAA VI International Colloquium on: Bluff Bodies Aerodynamics and Applications. Milano, Italy.

Grappe, G., Candau, R., Belli, A., Rouillon, J.D., 1997. Aerodynamic drag in field cycling with special reference to the Obree's position. Ergonomics 40 (12), 1299-1311.

Gross, A.C., Kyle, C.R., Malewicki, D.J., 1983. The aerodynamics of human-powered land vehicles. Scientific American 249 (6), 142-152.

Hanna, R.K., 2002. Can CFD make a performance difference in sport?. In: Ujihashi, S., Haake, S.J. (Eds.), The Engineering of Sport 4. Blackwell Science, Oxford, pp. 17-30.

Jeukendrup, A.E., Martin, J., 2001. Improving cycling performance – How should we spend our time and money. Sports Medicine 31 (7), 559-569.

Kim, S.-E., 2004. Large eddy simulation using unstructured meshes and dynamic subgrid-scale turbulence models. In Proceedings of the 34th AIAA Fluid Dynamics Conference and Exhibit, Technical Report AIAA-2004-2548. Portland, Oregon.

Kyle, C.R., 1991. The effects of crosswinds upon time trails. Cycling Science 3 (3-4), 51-56 (from Basset et al., 1999)

Kyle, C.R., Burke, E.R., 1984. Improving the racing bicycle. Mechanical Engineering 106 (9), 34-45.

Launder, B.E., Spalding, D.B., 1972. Lectures in Mathematical Models of Turbulence, Academic Press, London, England.

Lecrivain, G., Slaouti, A., Payton, C., Kennedy, I., 2008. Using reverse engineering and computational fluid dynamics to investigate a lower arm amputee swimmer's performance. Journal of Biomechanics 41 (13), 2855-2859.

Lukes, R.A., Chin, S.B., Haake, S.J., 2005. The understanding and development of cycling aerodynamics. Sports Engineering 8, 59-74.

Lukes, R.A., Hart, J.H., Chin, S.B., Haake, S.J., 2004. The aerodynamics of mountain bicycles: The role of computational fluid dynamics. In: Hubbard, M., Mehta, R.D., Pallis, J.M. (Eds.), The Engineering of Sport 5. International Sports Engineering Association, Sheffield.

Martin, J.C., Milliken, D.L., Cobb, J.E., McFadden, K.L., Coggan, A.R., 1998. Validation of a mathematical model for road cycling power. Journal of Applied Biomechanics 14, 276-291.

Mathey, F., Cokljat, D., Bertoglio, J.P., Sergent, E., 2006. Assessment of the vortex method for Large Eddy Simulation inlet conditions. Progress in Computational Fluid Dynamics 6 (1-3), 58-67.

Meile, W., Reisenberger, E., Mayer, M., Schmölzer, B., Müller, W., Brenn, G., 2006. Aerodynamics of ski jumping: experiments and CFD simulations. Experiments in Fluids 41, 949-964.

Padilla, S., Mujika, I., Angulo, F., Goiriena, J.J., 2000. Scientific approach to the 1-h cycling world record: a case study. Journal of Applied Physiology 89, 1522-1527.

Rouboa, A., Silva, A., Leal, L., Rocha, J., Alves, F., 2006. The effect of swimmer's hand/forearm acceleration on propulsive forces generation using computational fluid dynamics. Journal of Biomechanics 39 (7), 1239-1248.

Spalart, P.R., 2001. Young person’s guide to Detached-Eddy Simulation grids. NASA Contractor Report CR-2001-211032. NASA, Virginia.

Wilson, D.G., 2004. Bicycling Science. 3rd Ed. MIT Press, USA.

Wolfshtein, M., 1969. The velocity and temperature distribution in one-dimensional flow with turbulence augmentation and pressure gradient. International Journal of Heat and Mass Transfer 12 (3), 301-318.

Zaïdi, H., Taiar, R., Fohanno, S., Polidori, G., 2008. Analysis of the effect of swimmer's head position on swimming performance using computational fluid dynamics. Journal of Biomechanics 41 (6), 1350-1358.

Zdravkovic, M.M., Ashcroft, M.W., Chisholm, S.J., Hicks, N., 1996. Effect of cyclist’s posture and vicinity of another cyclist on aerodynamic drag. In Haake, S.J. (Ed.), The Engineering of Sport. Balkema, Rotterdam, pp. 21-28

Figure captions

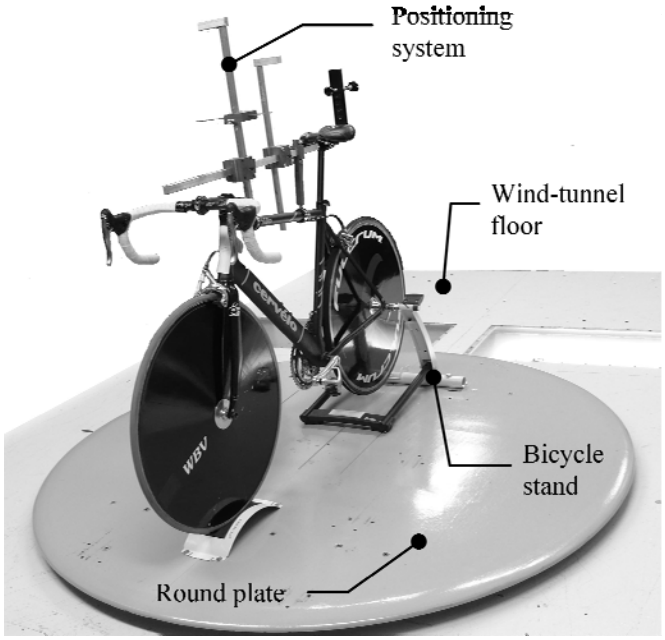

Figure 1: Bicycle test setup for wind-tunnel test.

Figure 2: Different cyclist positions: (a) Upright position (UP); (b) Dropped position (DP); (c) Time-trail position (TTP).

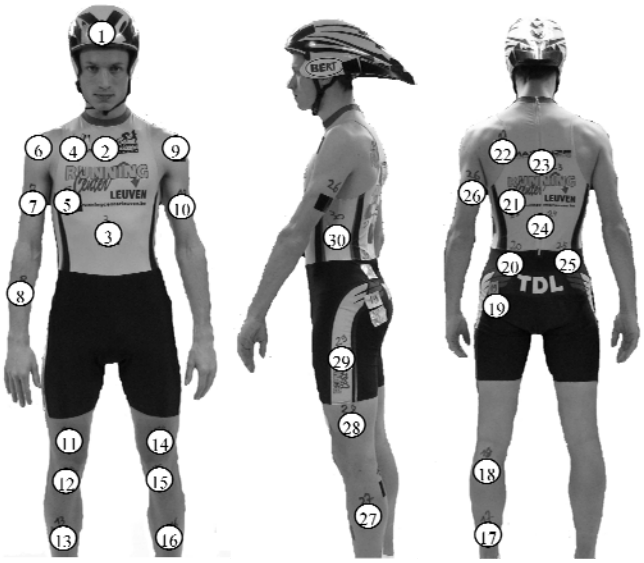

Figure 3: Locations of the pressure plates on the cyclist's surface (30 plates in total).

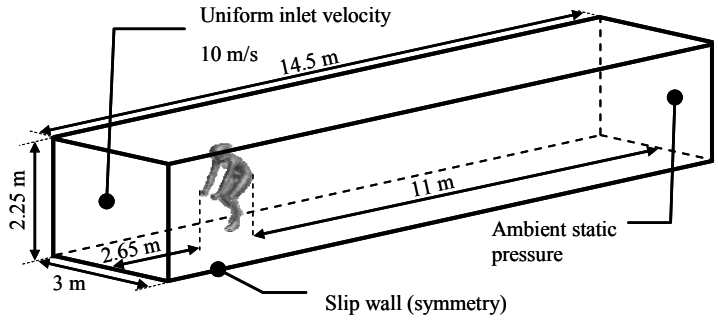

Figure 4: Computational domain and boundary conditions.

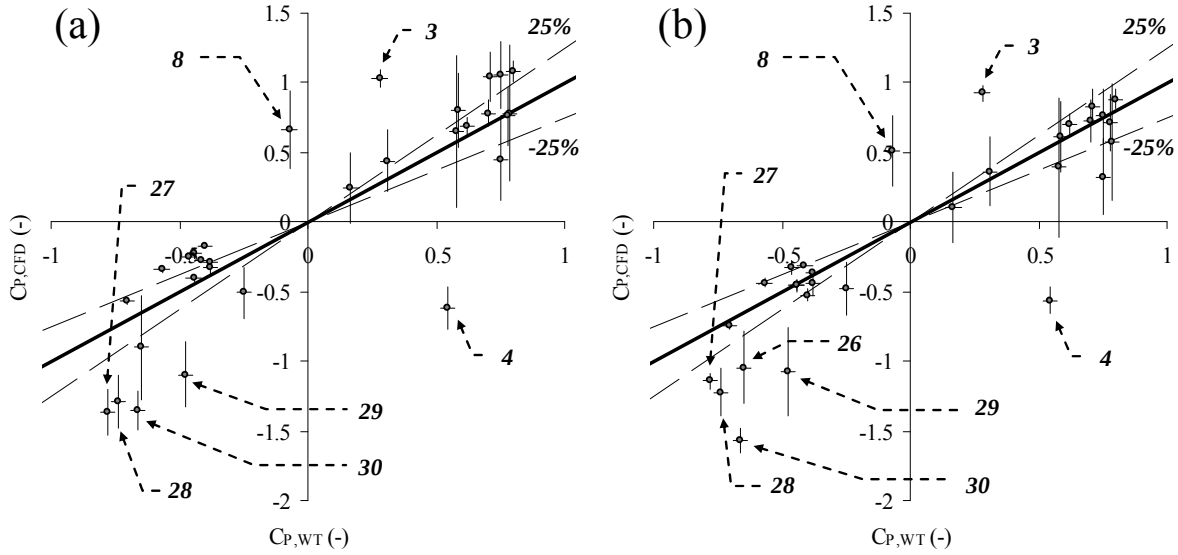

Figure 5: Comparison between pressure coefficients of wind-tunnel tests ($C_{P,WT}$) and CFD simulations ($C_{P,CFD}$) (with uncertainty bands) for the upright position (UP): (a) RANS simulations; (b) LES simulations. The uncertainty band for $C_{P,CFD}$ is the standard deviation from the averaged value within a circular zone (radius 2.5 cm) on the surface of the cyclist. For the uncertainty of $C_{P,WT}$, the measurement error on the pressure plates (7 Pa) is used. The dotted lines represent 25% deviation from the solid line.

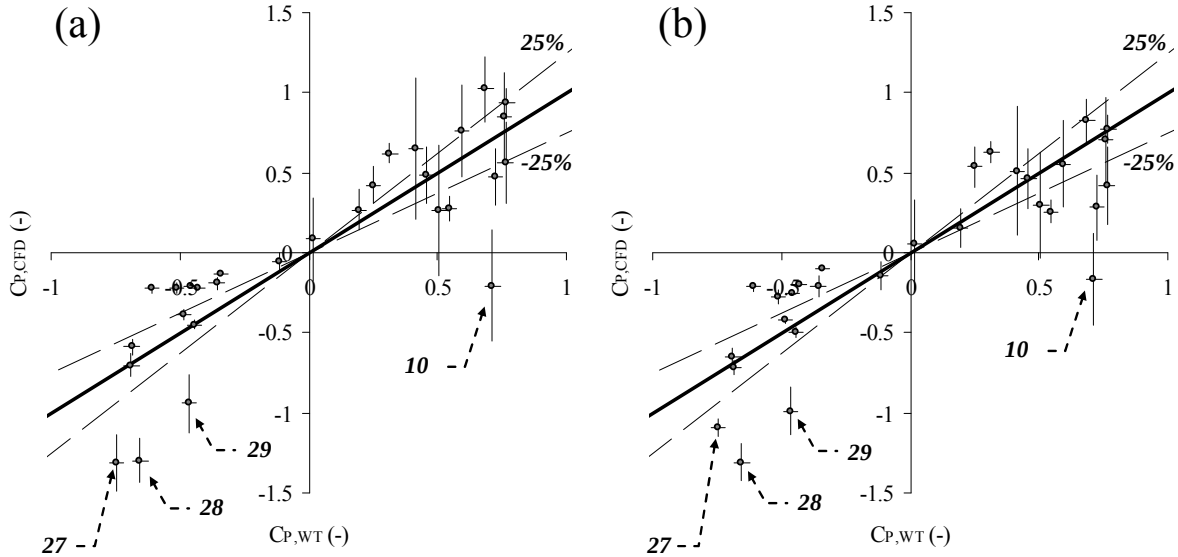

Figure 6: Comparison between pressure coefficients of wind-tunnel tests ($C_{P,WT}$) and CFD simulations ($C_{P,CFD}$) (with uncertainty bands) for the time-trail position (TTP): (a) RANS simulations; (b) LES simulations. The uncertainty band for $C_{P,CFD}$ is the standard deviation from the averaged value within a circular zone (radius 2.5 cm) on the surface of the cyclist. For the uncertainty of $C_{P,WT}$, the measurement error on the pressure plates (7 Pa) is used. The dotted lines represent 25% deviation from the solid line.

Table 1: Comparison of drag areas (for cyclist with bicycle) and other experimental details for several wind-tunnel experiments.

Author	Position ([a])	Wind speed U (m/s)	Drag area AC_D (m²)	Static/ Dynamic ([b])	Test section size (m)	Blockage ratio ([c])	Number of cyclists
Kyle and Burke (1984)	Dropped Crouched Hill descent	9-15.5	0.32 ([d]) 0.25 ([d]) 0.23 ([d])	Static	3x2.1	8%	1
Dal Monte et al. (1987)	Time-trail	15	0.246-0.254 ([e])	Static	9.6x4.2	1%	1
Kyle (1991) ([j,k])	Time-trail	13.3	0.221 ± 0.010 ([d,f])	Static	3x2.1	8%	3
Broker and Kyle (1995) ([k])	Time-trail	13.3	0.203 ± 0.012 ([d,f])	Static	-	-	5
Zdravkovich et al. (1996) ([j])	Upright Dropped Time-trail	± 8.2	0.26-0.38 ([g,h]) 0.23-0.34 ([g,h]) 0.17-0.23 ([g,h])	Static	2.2x1.6	14%	2
Martin et al. (1998)	Time-trail	13.4	0.269 ± 0.006 ([f])	Dynamic	3x2.1	8%	6
Padilla et al. (2000)	Time-trail	13.9	0.244	Static ([i])	-	-	1
Jeukendrup and Martin (2001)	Upright Dropped Time-trail	± 12.5	0.358 0.307 0.240-0.269 ([e])	Static ([i])	-	-	1
Gibertini et al. (2008) ([j])	Dropped Time-trail	13.9	0.275 0.223	Dynamic	4x3.84	3%	1
Garcia-Lopez et al. (2008) ([j])	Time-trail Time-trail	15	0.260 ± 0.024 ([f]) 0.341 ± 0.030 ([f])	Static Dynamic	3x2.2	8%	5

([a]) Upright: hands on upper part of a (standard) handlebar, Dropped: hands on lower (bent) parts of a (standard) handlebar and straight arms, Crouched: same as dropped but with bent elbows and crouched torso, Time-trail: time-trail handlebar and arms on elbow rests, Hill descent: hands on centre of upper handlebar and chin resting on hands; ([b]) Static: without pedalling and without rotating wheels, Dynamic: with pedalling and/or rotating wheel(s); ([c]) Calculated for frontal area (A) of 0.5m²; ([d]) For an air density of 1.206kg/m³; ([e]) Variation due to adjustments in position and/or equipment; ([f]) Average value and standard deviation; ([g]) Drag area without bicycle; ([h]) Individual values for cyclists; ([i]) According to Garcia-Lopez et al. (2008) (not reported in original paper); ([j]) More positions were reported in the paper but not mentioned here for the sake of brevity; ([k]) Data obtained from Basset et al. (1999).

Table 2: Drag area of cyclist and bicycle ($AC_{D,cyclist\ \&\ bicyle}$), drag area of cyclist ($AC_{D,cyclist}$) and ratio of these drag areas for different positions for the wind-tunnel experiments.

Position	$AC_{D,cyclist\ \&\ bicyle}$ (m²)	$AC_{D,cyclist}$ (m²)	$\frac{AC_{D,cyclist}}{AC_{D,cyclist\ \&\ bicycle}}$ (%)
UP	0.270	0.193	72%
DP	0.243	0.167	68%
TTP	0.211	0.134	64%

Table 3: Drag area of cyclist from CFD simulations ($AC_{D,cyclist,CFD}$) and differences with wind-tunnel experiments ($AC_{D,cyclist}$), i.e. without bicycle setup (see Table 2), for different positions for RANS and LES.

Position	Turbulence modelling	$AC_{D,\ cyclist,\ CFD}$ (m²)	$\frac{AC_{D,cyclist,\ CFD} - AC_{D,cyclist}}{AC_{D,cyclist}}$ (%)
UP	RANS	0.219	13%
	LES	0.219	13%
DP	RANS	0.179	7%
	LES	0.172	3%
TTP	RANS	0.150	12%
	LES	0.142	6%

Appendix 1: CFD simulations

Boundary conditions (see Figure 4)

At the inlet, a low-turbulent and uniform inlet velocity was imposed, namely 10 m/s with a turbulence intensity of 0.02%. Note that the distance of the inlet to the cyclist was chosen to be sufficiently large in order to have no pressure gradients in the inflow plane. Also note that the inflow conditions for turbulence for LES were specified by taking into account fluctuations (vortex method; Mathey et al., 2006). Due to the low turbulence level however, these fluctuations died out quite rapidly, i.e. before reaching the cyclist. Only the lowest wind speed (10 m/s) was evaluated in the simulations in order to limit the grid resolution in the boundary-layer region, since the required cell size near the cyclist's surface had to decreases with increasing wind speed in order to resolve the boundary layer appropriately with LRNM (Defraeye et al., 2010). The cyclist's surface was modelled as a no-slip boundary (i.e. a wall) with zero roughness. For the wind-tunnel walls, a slip-wall boundary (symmetry) was used in order to avoid resolving the boundary layer here, which would have required a high grid resolution close to these walls. Slip walls assume that the normal velocity component and the normal gradients at the boundary are zero, resulting in flow parallel to the boundary. At the outlet of the computational domain, the ambient static pressure was imposed.

Spatial and temporal discretisation

The grid is a hybrid grid, consisting of prismatic cells in the boundary-layer region on the cyclist's surface, tetrahedral elements in the vicinity of the cyclist and hexahedral elements further away from the cyclist, which results in a total amount of about 4.7×10^6 computational cells. The grid was built based on a grid sensitivity analysis according to best practice advice in CFD (Casey and Wintergerste, 2000). The average cell size in the wake region is 0.03 m. The y^+ values on the surface of the cyclist are below 3. For unsteady LES simulations, the temporal discretisation is dependent on the spatial discretisation. Both are related by the CFL (Courant-Friedrichs-Lewy) number:

$$\mathrm{CFL} = \frac{u\Delta t}{d} \tag{3}$$

where u is the characteristic velocity in the cell, Δt is the time step and d is the characteristic cell dimension. Time steps resulting in CFL numbers of 1 are suggested in the wake region (Spalart, 2001). For the simulations, the choice of the time step and averaging period was also based on a sensitivity analysis. A time step of 4.3×10^{-4} s was chosen, resulting in CFL numbers below about 1 in the majority of the domain, with maximal values not exceeding 5, and values of about 0.2 in the wake. A dimensionless simulation time of about 1.4 flow-through-times was found to be sufficient to obtain accurate averaged values for drag and surface pressures, where the flow-through-time (t_{FT}) is defined as:

$$t_{FT} = \frac{UT}{L_D} \tag{4}$$

where U is the free-stream (approach flow) wind speed (10 m/s), T is the averaging period (2 s) and L_D is the length of the computational domain (14.5 m).

Simulation parameters

The simulations are performed with the CFD package Fluent 6.3, which uses the control volume method. Steady RANS is used in combination with a turbulence model. The standard k-ε model (Launder and Spalding, 1972) is used together with low-Reynolds number modelling (LRNM) to take care of the viscosity-affected region, i.e. the boundary layer on the cyclist's surface, for which the one-equation Wolfshtein model (Wolfshtein, 1969) is used. Note that surface roughness values cannot be specified because LRNM is used to model the boundary layer. Although other k-ε models are available, the standard model is evaluated in this study since it is included in most commercial codes and it is used in most numerical studies in sports, which were mentioned in Section 1. For the LES simulations, the dynamic Smagorinsky subgrid-scale model is used (see Kim, 2004).

Second-order discretisation schemes are used throughout, except for momentum in LES simulations, for which a central differencing scheme is used. The SIMPLE algorithm is used for pressure-velocity coupling. Pressure interpolation is second order. For LES simulations, second-order implicit time stepping is used. For the RANS simulations, convergence was assessed by monitoring the velocity and turbulent kinetic energy on specific locations in the flow field, the surface friction on the surface of the cyclist and the resulting drag force on the cyclist. For the LES simulations, 20 iterations per time step were found to be sufficient to have convergence within a certain time step where the convergence behaviour was assessed in a similar way as mentioned for RANS.